Reduced graphene oxide for Li–air batteries
the effect of oxidation time and reduction conditions for graphene oxide

Storm, Mie Møller; Overgaard, Marc; Younesi, Reza; Reeler, Nini Elisabeth Abildgaard; Vosch, Tom; Nielsen, Ulla Gro; Edström, Kristina; Norby, Poul

Published in:
Carbon

Link to article, DOI:
10.1016/j.carbon.2014.12.104

Publication date:
2015

Document Version
Peer reviewed version

Reduced graphene oxide for Li-air batteries: The effect of oxidation time and reduction conditions for graphene oxide

Mie Møller Storm[a]‡, Marc Overgaard[a]‡, Reza Younesi[a], Nini Elisabeth Abildgaard Reeler[b,c,] Tom Vosch[b], Ulla Gro Nielsen[d], Kristina Edström[e] and Poul Norby[1a]*

[a]Department of Energy Conversion and Storage, Technical University of Denmark, Frederiksborgvej 399, 4000 Roskilde, Denmark, [b] Department of Chemistry, University of Copenhagen, Universitetsparken 5, 2100 Copenhagen Ø, [c]Sino-Danish Centre for Education and Research (SDC), Niels Jensens Vej 2, 8000 Aarhus C, Denmark, [d]Department of Physics, Chemistry and Pharmacy, University of Southern Denmark Campusvej 55, 5230 Odense M, Denmark and [e]Department of Chemistry-Ångström Laboratory, Uppsala University, Box 538, SE-75121 Uppsala, Sweden. ‡These authors contributed equally.

ABSTRACT:

Reduced graphene oxide (rGO) has shown great promise as an air-cathode for Li-air batteries with high capacity. In this article we demonstrate how the oxidation time of graphene oxide (GO) affects the ratio of different functional groups and how trends of these in GO are extended to chemically and thermally reduced GO. We investigate how differences in functional groups and synthesis may affect the performance of Li-O_2 batteries. The oxidation timescale of the GO

[1] Corresponding author: Tel: 0045 21 12 44 50. E-mail: pnor@dtu.dk

was varied between 30 min and 3 days before reduction. Powder X-ray diffraction, Micro-Raman, FE-SEM, BET analysis, and XPS were used to characterize the GO's and rGO's. Selected samples of GO and rGO were analyzed by solid state ^{13}C MAS-NMR. These methods highlighted the difference between the two types of rGO's, and XPS indicated how the chemical trends in GO are extended to rGO. A comparison between XPS and ^{13}C MAS-NMR showed that both techniques can enhance the structural understanding of rGO. Different rGO cathodes were tested in Li-O_2 batteries which revealed a difference in overpotentials and discharge capacities for the different rGO's. We report the highest Li-O_2 battery discharge capacity recorded of approximately 60,000 mAh/g_{carbon} achieved with a thermally reduced GO cathode.

1. INTRODUCTION:

Lithium-air (Li-O_2) batteries hold the promise for a future generation of rechargeable batteries with very high specific capacities. The development of such batteries is important for the future of green technologies. However, promising as these batteries are, much research is still needed, and many challenges must be overcome [1, 2]. Some of the issues in the future development of Li-air batteries are: Exploration of stable electrolytes suited for the highly reactive environment [3-5], lowering of the significant overpotential on charging the battery [6, 7] and improving cyclability [1]. In addition to these challenges the effects of possible contamination from the air should also be considered [8, 9]. Development of a stable and lightweight air-cathode for Li-air batteries is important to achieve its potential. Ottakam *et al* [10] tested isotope labeled ^{13}C as cathode material and found that not only the electrolyte decomposes upon cycling. Carbon may react as well, and the degree of reaction depends on the hydrophobicity of the carbon material. A capacity retention above 98% upon cycling in 0.5M $LiClO_4$ DMSO has been reached with TiC [11], electrodes made by vertical aligned N-doped coral-like carbon fibers has shoved high

cyclability combined with a high discharge capacity [12], and cathodes of woven carbon nanotubes also displayed high cyclability, both in regards to capacity limited cycles but also for deep discharged cycles[13].

Reduced Graphene Oxide (rGO) has shown great promise as an air-cathode with high capacity [14, 15] and the material has many of the abilities desired for the Li-air cathode; it has a high specific surface area and a good conductivity[16]. rGO may be prepared with a unique 3D morphology of interconnected pores with sizes on the nano- and mesoscale as well as a structure which is believed to lead to high capacities for graphene cathodes [14]. Several different types of related rGO have been tested as the Li-air battery cathode material, such as "normal" rGO [14, 15], doped rGO [17, 18], and metal containing rGO [19-22]. rGO cathodes have been tested for both the aprotic [14, 15] and hybrid [23] Li-air battery systems with promising results.

Even though rGO has been investigated [16, 24, 25], the difference of the functional groups in the graphene oxide (GO) and their relation with the functional groups in rGO has not been explored in detail. Gaining a deeper insight into these properties is important since they may have an influence on the use of rGO as a Li-air cathode material. We have investigated the effect of oxidation time on the structure and properties of GO as well as related thermally and chemically reduced GO. Different rGO's were tested as cathode materials for an aprotic Li-O_2 battery.

GO was prepared by a modified Hummers method [26] and the oxidation time for the GO synthesis varied between 30 min and 3 days. Chemically and thermally reduced GO was synthesized from the GO samples. Samples were characterized by Field Emission Scanning Electron Microscopy (FE-SEM), Brunauer–Emmett–Teller surface area analysis (BET), coupled Thermogravimetric Analysis and mass spectrometry (TGA-MS), X-ray powder diffraction

(XRD), micro-Raman spectroscopy, X-ray photoelectron spectroscopy (XPS), and solid state ^{13}C nuclear magnetic resonance spectroscopy (^{13}C-MAS NMR). Cathodes of selected rGO materials and cathodes of conductive carbon black Super C65 were tested and compared in Li-O_2 cells.

This study shows how some of the functional groups in GO relate to the functional groups of the synthesized rGO, and how the differences in rGO cathodes affects both discharge capacity and the overpotential for time limited discharge/charge cycling in a Li-air battery.

2. EXPERIMENTAL:

2.1. GO and rGO Preparation

GO was synthesized according to the modified Hummer's method [26]. In an Erlenmeyer flask on ice 3 g natural flake graphite, 325 mesh, with 99.8 % metals basis (Alfa Aesar) and 1.5 g $NaNO_3$ was mixed under stirring in 100 ml concentrated H_2SO_4. 12 g $KMnO_4$ was added very slowly to the still cooled Erlenmeyer flask and cooling was continued for 2 hours. The solution was then heated in a water bath to 35˚ C for the desired and variable time range (30 min, 1 hr, 3 hrs, 1 day, and 3 days). After heating, the solution was placed on ice and 100 ml ice-cooled water was added followed by slow addition of 25 ml 30% H_2O_2. The precipitate was isolated by centrifugation, washed with 0.1 M H_2SO_4 and left to vacuum dry at 25 ˚C overnight. GO was washed by centrifugation, four times with 1 M HCl followed by drying, and four times with acetone and drying in a vacuum furnace at 25 ˚C. The GO materials were named GOX (X=30min, 1H, 3H, 1D or 3D, denoting the oxidation time).

HyrGO synthesis, following [27]: 0.2 g GO was delaminated in 200 ml water by sonication for at least 1 hr and the solution was filtered on a Büchner funnel with filter paper. To a round

bottom flask containing the delaminated GO 2 ml of hydrazinium hydroxide was added. The solution was then heated under reflux at 100 °C for 24 hrs, causing precipitation of rGO. The solution was filtered and the rGO was washed with 5*100 ml milliQ water and 5*100 ml MeOH. The rGO was dried in air overnight and furthermore dried in an oven at 90 °C overnight.

TrGO synthesis, slightly modified from [28]: 0.2 g GO was placed in an alumina boat and inserted into a 50 mm (inner diameter) 1m long quartz tube was flushed with argon. Hereafter the tube was inserted into a tube furnace pre-heated to 1100 ˚C and shock-heated for 2 minutes. The quartz tube was extracted, cooled, and the TrGO powder was washed out with acetone. The rGO samples was named TrGOX or HyrGOX (X=30min, 1H, 3H, 1D or 3D, denoting the oxidation time of the GO).

2.2. GO and rGO characterization

FE-SEM was carried out on a Carl Zeiss Supra-35 instrument, 2kV was used for GO and 3-10kV for imaging rGO. BET Surface area was measured on a Quantachrome Autosorb-1 instrument and a Micromeritics ASAP 2020 with degassing times from 15-30 hrs at 120 ˚C (TrGO 300 ˚C).

TGA-MS was performed using a NETZSCH, STA 409CD TGA system coupled with a NETZSCH, QMS 403D MS system with approximately 15-20 mg of GO, inert argon flow and 0.5 C/min. XRD spectra were measured on a BrukerD8 between 5-80˚ in 2θ with a step size of 0.014˚ in 2θ and a step time of 1.9 seconds. The Li-air cathodes were cleaned and dried in a glovebox and measured in an air tight dome containing an Ar atmosphere. Micro-Raman spectroscopy was performed on a home build Micro-Raman set-up described in supplementary information. Raman data were fitted to a Lorenz function to the D and the G peak [29], see

supplementary information. The areas under the curves were used to calculate I(D)/I(G). XPS spectra were recorded on a commercial in-house PHI 5500 spectrometer with monochromatic Al K radiation. Scans were made with a step size of 0.1 eV and 50 to 80 repeated cycles. Igor Pro [30] was used for spectral analysis. XPS on cathodes was performed after cleaning them with dried DME and drying in a glovebox. A single cathode was removed from the battery and soaked in electrolyte for four days and cleaned prior to XPS measurement. Solid-state ^{13}C MAS NMR was performed at 11.7 T (125.6 MHz) using a 3.2 mm MAS NMR probe. Single pulse ^{13}C MAS NMR spectra (quantitative) were recorded using 15 kHz spinning speed. ^{13}C NMR spectra are referenced to TMS using the CH resonance in adamantane ($\delta(^{13}C)$ = 38.3 ppm) [31]. Four samples (GO30min, GO3D, TrGO30min and TrGO3D) were investigated by solid-state NMR (SSNMR) spectroscopy. MestreNova software was used for the analysis of the data and the assignment of the ^{13}C resonances is based on earlier published $\delta(^{13}C)$ in GO [32] and liquid state NMR shifts [33].

2.3. Battery tests

Samples of conductive carbon black Super C65 from Timcal and HyrGO (30min and 3D), respectively, were mixed for cathodes with polyvinylidene flouride (PVDF) in a 9:1 weight ratio in N-methyl-2-pyrrolidone (NMP) and drop-casted on cleaned stainless steel (SS) mesh (cleaned by 1 hr sonication in 2M H_2SO_4, followed by washing in water and acetone). TrGO (30min and 3D) was mixed with PVDF in a 1:1 ratio and drop-casted on cleaned SS-mesh. Different binder to carbon material ratios were used as the TrGO samples required more binder to work as cathode in the battery. The cathodes had an average weight of 1.4 mg for HyrGO, 0.9 mg for TrGO cathodes (the cathode of the highest measured specific capacity had a lower weight of 0.37

mg) and 0.9 mg for the Super C65 cathodes. The cathodes were dried in a vacuum oven in the glovebox at 80 ˚C for 12 hrs. The size of the square-like drop-casted cathodes was 4 x 4 mm. Paint-casted cathodes of TrGO samples were made by painting a thick slurry on cleaned SS mesh. The cathodes were dried in a vacuum oven in the glovebox at 80 ˚C for 12 hrs. The paint-casted cathodes had an average size of 50 mm^2 and an average weight of 0.7 mg. Li-O_2 batteries were assembled in a glovebox using a custom built Swagelok cell with gas volume of 10 ml. The batteries consist of a 10 mm Li-disk as the anode followed by two, EtOH cleaned and dried, Cellgaard membranes, 70 µl 1M LiTSFI in DME electrolyte [34], the cathode on the stainless steel mesh and additional 140µl electrolyte. The Swagelok cell was activated with oxygen by flushing 4 x 20 sec at a flow of approx. 2 ml/sec and an overpressure of 0.8 bar. The battery was disassembled, after flushing with argon, in the glovebox and the cathodes were carefully washed with dried DME. At least 3 drop-casted cathode batteries were tested with a current of 0.1 mA/cm^2 for capacity calculations. The cell test consisted of 3 hrs OCV, 5 min discharge, an impedance measurement (EIS), 9 hrs and 55min (or 2V discharge), 10 hrs (or 4.65V) charge, EIS, 2 cycles (10 hrs or 2-4.65V), followed by a deep discharge to 2V. Cycled batteries were charged and discharged between 2 and 4.65 V at 0.1 mA/cm^2 for 10 cycles.

3. RESULTS AND DISCUSSION:

This section describes the characterization of the GO and rGO samples by SEM, BET, TGA-MS, XRD, and micro-Raman spectroscopy, followed by the XPS and ^{13}C MAS-NMR results, as both techniques give insight into the functional groups in the samples. After GO and rGO characterizations selected rGO samples are evaluated as cathode materials for Li-O_2 batteries together with cathodes of Super C65 carbon black.

3.1. CHARACTERIZATION OF GO AND rGO

The different GO's in this article are denoted GOX (X denotes the GO oxidation time as being 30min, 1H, 3H, 1D or 3D, H = hour(s) and D = day(s)). The notation for the chemically reduced rGO, reduced by the hydrazine hydrate method [27], is HyrGOX and for the thermally reduced rGO [28] it is TrGOX (X = 30min, 1H, 3H, 1D or 3D).

Figure 1 shows selected SEM micrographs of GO and rGO. Figure 1a is a SEM micrograph of GO30min. SEM micrographs of the other GO samples showed very similar morphology c.f. Figure S1.

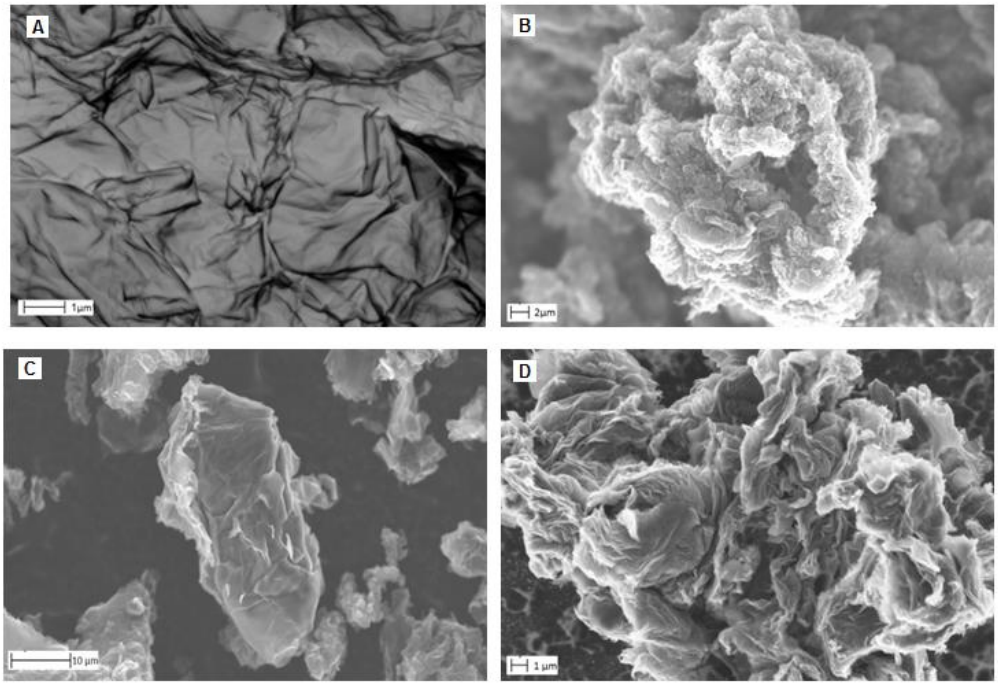

.

Figure 1: SEM micrographs of (A) GO30min, (B) HyrGO3D, (C) and (D) TrGO3D. SEM micrographs reveal different morphologies with an interconnected porous network for the rGO samples.

The SEM micrographs of GO reveal a flat crumbled surface with very few or no penetrating cavities. SEM images of HyrGO3D (Figure 1b) and TrGO3D (Figure 1c, 30sec reductive heating and Figure 1d, 2 min reductive heating) indicate two different types of morphologies. The HyrGO morphology resembles small aggregates, which may be formed by aggregation in the solution during the reduction process. During the hydrazine reduction GO changes from water-soluble to hydrophobic HyrGO which leads to an observable large scale aggregation. These aggregated structures have cavities and a number of crumpled layers. TrGO3D in figure 1c shows small flat particles with a surface resembling "folded sheets". However, Figure 1d points to a slightly more crumbled structure, but somewhat similar to the aggregate morphology seen for the HyrGO3D. Both TrGO and HyrGO SEM pictures show indications of morphologies with a porous network. No great difference in morphology was observed for the different time dependent oxidized samples.

The BET surface areas of the HyrGO samples ranged from 353 to 497 m^2/g with no observable correlation with the oxidation time. The surface areas of TrGO were of similar size ranging from 343 to 484 m^2/g. However, the surface area of the TrGO's followed a trend where increased oxidation time led to a larger surface area. (Table S1 reports the BET values of HyrGO and TrGO, supplementary information). These increased surface areas might be explained by an increasing amount of edges and defect formations in the graphene induced by the prolonged oxidation time and the subsequent reduction method.

TGA-MS was measured for GOX (X = 30min, 1H, 1D and 3D), with similar results for the different oxidized samples. An initial small loss of mass was observed from 25-110 °C followed by a substantial 48%, 52%, 52%, and 58% loss of mass for GO30min, GO1H, GO1D, and GO3D, respectively from 110-210 °C. This was again followed by a small loss of mass up to

1050 °C. The loss of CO_2 is caused by the thermal reduction of GO. The dramatic loss of mass corresponded to loss of H_2O and CO_2. At 1050 °C the total remaining mass was 34%, 29%, 28%, and 22% of the initial mass for GO30min, GO1H, GO1D, and GO3D, respectively, indicating an increase in functional groups or/and more intercalated water molecules as the oxidation time is increased. See the TGA-MS measurements in Figure S2.

The five different GO powders has the well-known GO XRD patterns (Figure 2) and Raman spectra (selected spectra are shown in Figure 3).

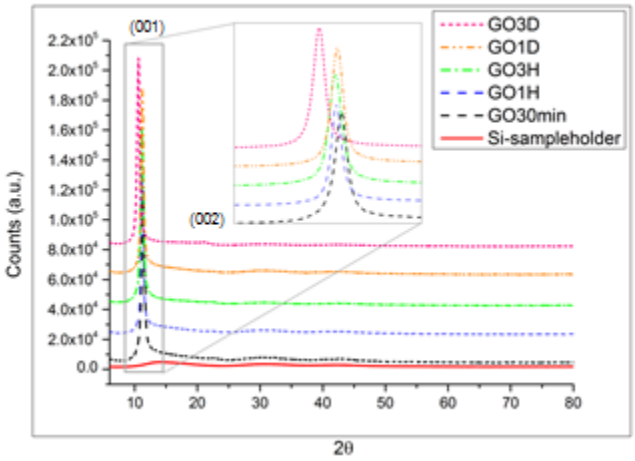

Figure 2: XRD of GO30min-GO3D showing an increasing d-spacing of the graphene layers as a function of oxidation time. The inset shows an expansion for the region of the first reflection.

The GO diffraction patterns of oxidation time GO1H to GO1D have their interlayer distance ((001) reflection)[2] between 11.19 and 11.22° (d ≅ 7.9 Å), whereas the GO30min showed a

[2] For the GO and GO derived materials we have indexed the patterns based on a hexagonal unit cell where the c-axis is equal to the interlayer distance

somewhat smaller distance between the graphene layers with the (001) reflection at 11.36˚ in 2θ (d = 7.78 Å). GO3D has a greater interlayer distance, d = 8.44 Å, which may be explained by a higher degree of water absorption or functionalization. TGA-MS supports this as GO3D has the highest loss of mass. Ref [35] shows that intercalation of water in GO has an influence on the d-spacing, as an approximately 6% change in the relative humidity in air can downshift the main peak with 0.5°. This indicates that intercalated water could have a similar effect on the d-spacing. Furthermore, the GO3D diffractogram shows a weak second order reflection at 20.82˚ (d = 4.26 Å). The chemically reduced rGO (HyrGO) XRD diffractions show a broad (001) reflection around 24˚ (d ≅ 3.7 Å) whereas the thermally reduced rGOs (TrGO) have the (001) reflection at 24˚ (d = 3.7 Å) for TrGO30min and 26.1-26.4˚ (d ≅ 3.4 Å) for TrGOX (X = 1H, 3H, 1D, and 3D). XRD diffractions of TrGO and HyrGO can be seen in Figure S3. These reflections resemble the (002) reflection of graphite but with larger interlayer distances. The distance between the graphene layers are slightly greater for the HyrGOs compared to the TrGO. Both the HyrGO and the TrGO diffraction patterns display the (100) reflection around 43˚. The HyrGO diffraction peaks are narrower than those of TrGO which indicates a higher crystallinity.

Figure 3 shows a representative Raman spectra of graphite, GO, HyrGO, and TrGO (Additional Raman spectra and data of TrGO and HyrGO can be found in supplementary information; Table S2, Figures S4 and S5).

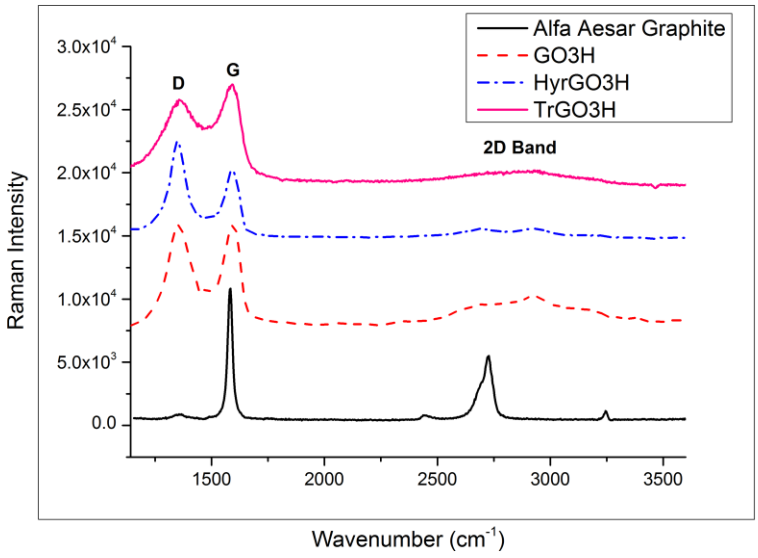

Figure 3: Raman spectra of graphite, GO3H, HyrGO3H, and TrGO3H demonstrate distinct differences between GO, HyrGO and TrGO. The D, G, and 2D bands are indicated in the figure on the spectra.

Micro-Raman spectroscopy showed a definitive and clear difference between graphite, GO, and the two different HyrGO and TrGO samples. The D band at approximately at 1350 cm^{-1} and the G band around 1590 cm^{-1} are of a very similar intensity for the GO samples. Previously Hiramitsu *et al.* [36] observed a peak around 1750 to 1850 cm^{-1} related to C=O vibrations [29]. The Raman spectra of our GO samples display a tendency to a very small shoulder in the area of 1840 cm^{-1}, although the signal is too weak to make any definitive conclusion. The Raman spectra of HyrGO have a lower but broader G peak compared to the D peak and a larger I(D)/I(G) ratio as compared to the GO samples. The ratio of I(D)/I(G) is often reported as a measure of the disorder in the carbon material [16, 37], thus the D peak represents the lack of order in the initial graphitic sp^2 plane (G peak). We would expect a decrease in the I(D)/I(G) ratio upon reduction if

we restore the graphene sheet, however this is not observed. Similar results have been reported earlier [38] and were explained by creation of graphitic domains in rGO, of which there are more domains but of smaller domain size than in GO. The TrGO's spectra show a high G peak compared to the HyrGO spectra and has an I(D)/I(G) ratio larger than for both HyrGO and GO. The TrGO Raman spectra display features also seen in amorphous carbon, but this tendency is not observed in HyrGO. Micro-Raman could not detect large differences between the HyrGO or TrGO samples which had been made from GO using different oxidation times, see supporting information table S2 and S5.

XPS measurements of the GO samples demonstrated the presence of carbon and oxygen on the surface as well as minor impurities of chlorine and sulfur from the synthesis method. The impurities were not detected in any of the rGO samples. Somewhat similar relative surface concentrations of carbon and oxygen (C/O ratio) for the GO samples were observed indicating that an oxygen saturation of the graphene framework is quickly reached. The C1s spectra of GO had different shapes depending on the oxidation time and were deconvoluted with the expected binding types being C-C, C-O, C=O, and C(O)O, as in ref [39]. A variation of ±0.1 eV for the binding energies were accepted for the XPS deconvolution for all samples. The relative contribution of each bond to the C1s spectra of GO are shown in Figure 4 (these results are also presented in Table S3). More GO spectra and the relative amounts of deconvolved peaks can be found in supplementary information, Table S3 and Figure S6. The C-C graphitic backbone is clearly affected by the oxidation time. As the oxidation time increases the relative amounts of pure C-C bonds decreases from a ratio of 69% (GO30min) to 51% (GO3D). The relative amount of C-O bindings increase from GO30 min (25%) to GO3D (36%) as does the relative amounts of C=O and C(O)O bonds. The increase of C=O and C(O)O could indicate a destruction of the

carbon backbone as these functional groups are expected to be situated at the edges of the graphene sheet. The C1s spectra of TrGO were deconvoluted with the expected binding types of C-C, C-O, C=O, and C(O)O and the HyrGO spectra were deconvoluted with expected binding types of C-C, C-N, C-O, C=O, and C(O)O following results reported earlier by Stankovich *et al.* [27].

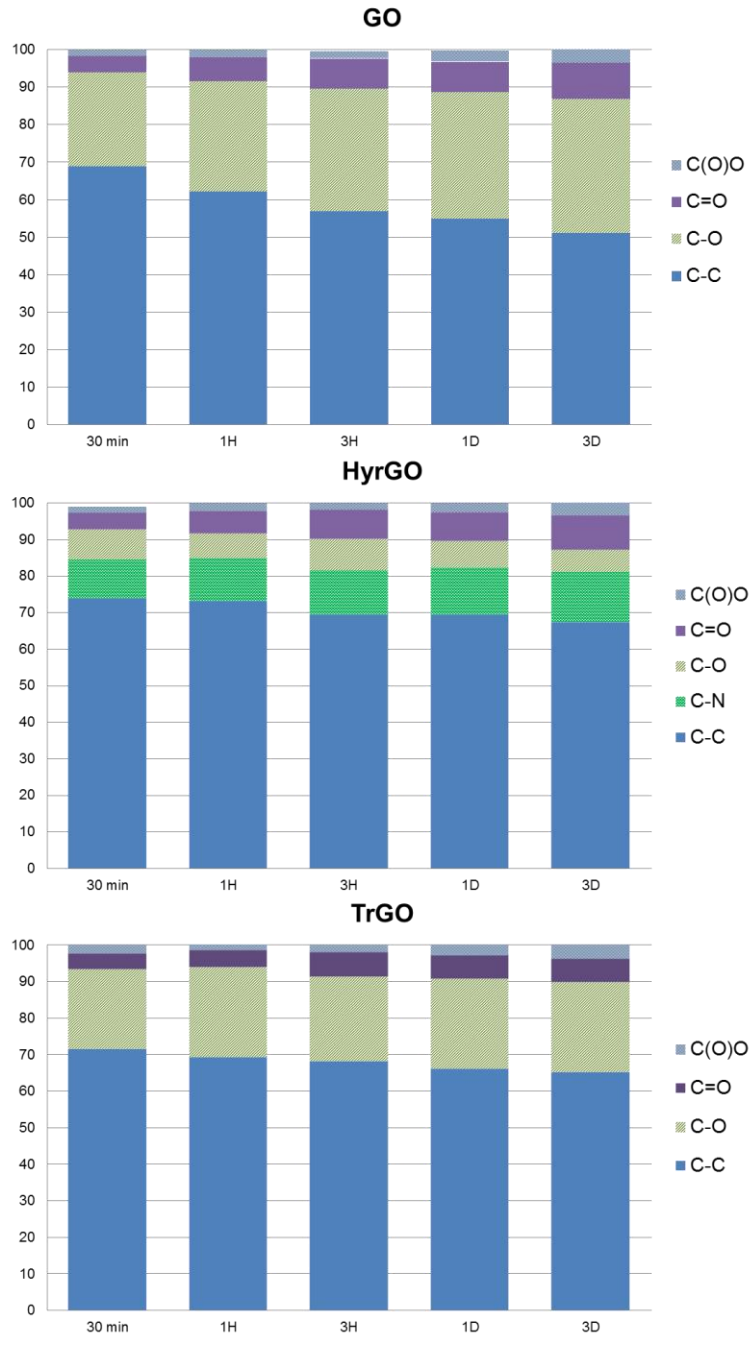

Figure 4: The relative contribution of each bond calculated based on the deconvoluted C1s spectra illustrating the evolution of the functional groups for GO, HyrGO, and TrGO. XPS results indicate that selected functional group trends from GO are inherited by HyrGO and TrGO.

The survey scans of HyrGO revealed the presence of nitrogen from attached hydrazine as well as a much higher C/O ratio compared to GO between 19.8 and 11.8. Both results were in agreement with previous studies [27]. Deconvolution of the C1s spectra for the HyrGO samples (Figure S6) were performed with a set of chemical guidelines to achieve a high chemical accuracy in the result, see supplementary information. The relative contribution of each bond type to the C1s spectra of HyrGOs are seen in Figure 4. Similarly as for the GO samples the HyrGO C1s spectra show how the C-C bond of the rGO decreases from 74% to 67% as the oxidation time is increased. The percentages of C-C bond are greater for the HyrGO samples than for the GO samples, which can be explained by removal of functional groups. The trend for the C=O and C(O)O groups are similar as for the GO samples, but this is sensitive to by the deconvolution guidelines. The amount of C-N bonds in the HyrGO samples grow with increased oxidation time from 11 to 14%. This increase in nitrogen is also observed when the elemental quantities from the survey scans are compared. The elemental quantities show a small amount of nitrogen (approx. 2.5-4 %). The increase in hydrazine bonding to the graphene plane can be explained by an increase in epoxy groups (C-O-C) of the GO as the oxidation time is increased [27, 40]. This effect demonstrates that the increasing amounts of C-O groups in GO is carried through to HyrGO. The trends seen for the C-C and C-O bonds in GO seems to be transferred to the HyrGO samples.

The C1s spectra of TrGO (Figure S5) were fitted with the peaks of C-C, C-O, C=O, C(O)O, and π-π^*. The relative contributions of each bond to the deconvoluted spectra of TrGO are summarized in Figure 4. The ratio of C-C bonds decreases with increased oxidation time from 72 to 65%, as are also observed for HyrGO and GO. There is a higher ratio of C-C in the TrGO compared to the GO samples. The ratio of C-O bonds after thermal reduction does not seem to

depend on the GO functionality as the ratio is similar for all five samples. The ratios of C=O are slightly decreased and the C(O)O functional groups are similar as compared to those of GO, and the TrGO samples seem to adopt the GO trend where increased oxidation time leads to increased amounts of C(O)O bonds. The C=O is increasing up to TrGO3H. The trends seen in GO for C-C, C=O, and C(O)O seems to be extended to the TrGO samples.

Comparison of the HyrGO and TrGO measurements reveals that the ratio of C-C bond is in the same range with a slightly higher ratio of C-C bond in the HyrGO samples. There is a much higher ratio of C-O in the TrGO, but the HyrGO samples contain C-N bonds. The ratio of the edge bonded groups C=O and C(O)O are similar.

Solid state ^{13}C MAS NMR was performed on four samples of GOX and TrGOX (X = 30min and 3D), see Figure 5. They show a slightly different result than XPS in terms of functional groups. However, it is important to note that SSNMR reflects the average composition of the sample, whereas XPS is a surface sensitive technique. Furthermore, regions near paramagnetic centers may be invisible due to fast relaxation such centers have recently been identified in GO [41].

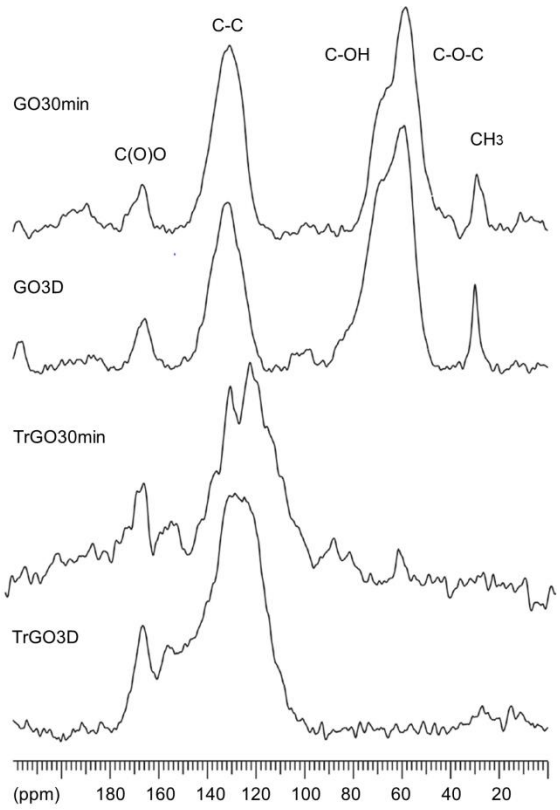

Figure 5: Solid state ^{13}C MAS NMR spectra of selected GO and TrGO samples with the isotropic chemical shift regions for the different functional groups indicated.

^{13}C MAS NMR of the GO samples showed the presence of C(O)O, C-C, C-OH, C-O-C, and CH_3 groups. If the methyl group is ascribed to the washing solvent, acetone, the identification is very similar to the XPS results for GO. The NMR results for the GO samples are very similar, see Table 1, the major resonances are aromatic C from the graphene sheet, denoted graphitic in the table, hydroxyl (C-OH) and ether/alkoxy (C-O-C) groups, which together constitute 90 % of the sample. There are different graphitic signals in the table originating from slightly different environments. In addition, smaller components are C(O)O (from an ester or acid group) and CH_3, assigned to acetone (residual solvent). The concentrations of the different functional groups

calculated from XPS and ^{13}C-NMR are not identical, but as both measurements resulted in broad spectra this is not unexpected. However, both XPS and ^{13}C-NMR show a decrease in the amount of C-C bond upon oxidation and an increasing amount of C-OH and C(O)O. However, according to the XPS C-O increases with oxidation time whereas the ^{13}C-NMR displays the opposite tendency. The ^{13}C-NMR does not detect any C=O bonds, with an expected chemical shift around 190 ppm, but these may be below the detection limit (3-5%). The sample composition significantly changes upon reduction. The aliphatic C-O-C and C-OH groups disappear and the regions for C=C, aromatic C and carbonyls at 100-180 ppm becomes more complicated implying the presence of many different local environments. These have been assigned in Table 1. ^{13}C-NMR of the TrGO samples did only reveal small or zero traces of C-OH and C-O-C groups. These groups were clearly visible, as C-O in the XPS spectra. A similar disagreement between XPS and ^{13}C-NMR has been seen for GO and rGO synthesised by Lawsons reagent by Liu *et al* [42]. However, the ^{13}C-NMR spectra of rGO show the formation of two new functional groups compared to the GO: A sp^2 carbon single-bonded to an oxygen atom and a lactol group. The table for TrGO3D does not have the C_{sp2}-O listed, but the broad O=C-O signal at 156.3 ppm may be split into O=C-O and the C_{sp2}-O functionality, with the concentration being split roughly in half. The lactol group was detected by Ayajan *et al* [32] in GO and is a heavily substituted 5 or 6 membered-ring formation. If these types of structures are formed during the heating, they can explain the presence of C-O groups in XPS as well as the formation of the new groups in ^{13}C-NMR. ^{13}C-NMR shows a decrease in the amount of graphitic signals from TrGO30min to TrGO3D agreeing with the XPS result. With the splitting of the 156.3 ppm peak in TrGO3D, under the assumption of the formation of lactol groups, the amounts of the C-O functionalities are comparable to the XPS results. The amount of C(O)O groups detected with ^{13}C-NMR is

much greater than those detected with XPS, but these signals were difficult to assign precisely both in the XPS and NMR spectra.

Table 1: NMR results from analysis of the ^{13}C NMR spectra of GO30min, GO3D, TrGO30min, and TrGO3D.

Sample	**Assignment**	**δ_{iso} (ppm) ± 1 ppm**	**Conc. (%) ± 3%**	**Comment**
GO30min	O=C-O	166.5	5.3	Ester or acid-derivative
	”Graphitic”	131.2	41.3	
	C-OH	70.1	11.1	
	C-O-C	59.0	38.7	
	-CH_3	29.1	3.5	
GO3d	O=C-O	167.5	4.8	
	”Graphitic”	133.0	32.6	
	C-OH	67.9	33.0	
	C-O-C	58.2	25.3	
	-CH_3	29.9	4.3	
TrGO30min	O=C-O	166.9	12.2	Ester or acid-derivative
	O=C-O	156.2	3.7	
	C_{sp2}-O-	147.6	10.3	Aromatic C with O-substituent
	”Graphitic”	130.1	36.0	
	”Graphitic”	119	22.7	
	-C=C-	109.2	2.8	
	Lactol O-C-O	104.6	12.3	

TrGO3d	O=C-O	167.6	4.5
	O=C-O	156.3	19.7
	”Graphitic”	138.2	11.0
	”Graphitic”	132.4	8.9
	”Graphitic”	125.8	17.3
	”Graphitic”-C=C-	119.8	17.0
	-C=C-	112.3	11.0
	Lactol O-C-O	104.4	1.8
		92.6	6.3
	C-OH	66.1	1.5

3.2. rGO Li-AIR BATTERIES:

Figure 6 shows a battery test for one of the TrGO3D cathodes. The battery test consisted of three limited cycles (limited by 10 hours or 2-4.6 V) followed by a deep discharge. The three cycles, limited by time, were made to ensure that the cathodes could both be charged and discharged. The battery tests showed that all tested materials could be cycled within the limits of the test.

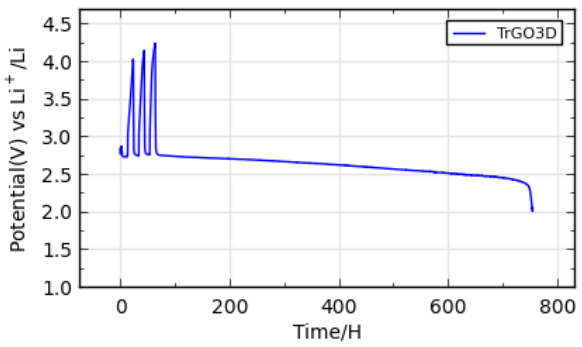

Figure 6: Battery test of a TrGO3D cathode tested at 0.1 mA/cm2.

A TrGO30min cathode was characterized by XRD in Ar atmosphere after deep discharge, see Figure 7. The presence of Li_2O_2 in the diffraction pattern confirmed that the desired Li-O_2 reaction had taken place. No crystalline carbonate species were detected showing that under these conditions there is no evidence of crystalline decomposition products of either electrolyte or cathode. XPS on a tested and cleaned cathode showed the formation of Li_2O_2 (Figure S7). A similar XPS result was obtained on a cathode which after battery test termination had been stored in electrolyte for several days. No lithium carbonate was detected on the cathodes.

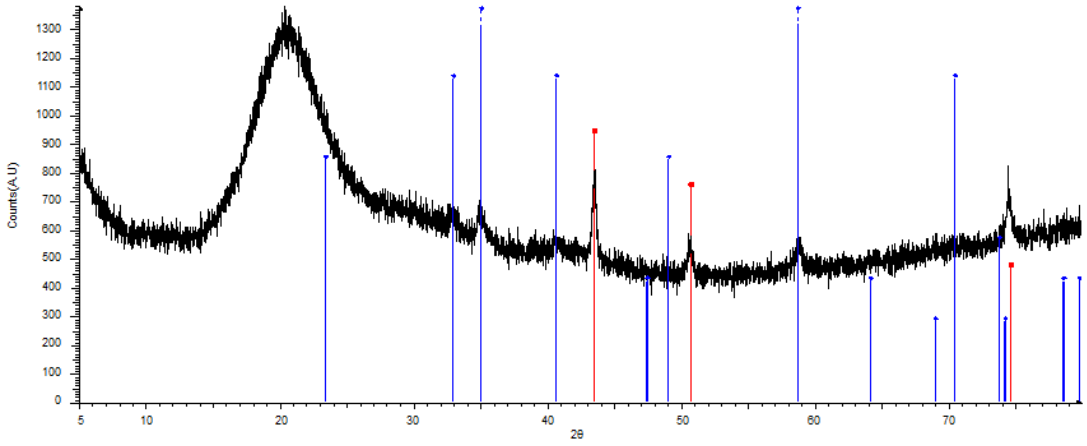

Figure 7: XRD of deep discharged TrGO30min battery cathode with peak assignment: blue = Li_2O_2 and red = SS mesh, FeNi. The XRD diffractogram shows only reflections from crystalline Li_2O_2 and no carbonate formation is observed.

The TrGO3D battery tested in Figure 6 has a capacity of 59,792 mAh/g_{carbon} (total cathode weight 0.37 mg), which is the largest capacity currently measured for a porous air-cathode for Li-air. Under the assumption that the cathode has a surface area of 300 m^2/g and is completely

covered with a uniform layer of Li_2O_2 the thickness of the layers is calculated to approximately 72 nm. This large capacity was only measured once. However, the other tested cathodes of this material had the highest average capacity of all the tested cathodes in this study. It was possible to cycle this battery but only with considerable loss of capacity as the first cycle was discharged for approximately 59,792 mAh/g, 692 Hrs, then recharged to ~15500 mAh/g (180 Hrs). The following cycles were deep discharged to an approximate specific capacity of 5931, 2414, 1491, 970 and 631 mAh/g_{carbon} (60, 28, 17, 10 and 5 Hrs). It was also possible to cycle the HyrGO3D cathodes, which resulted in four complete deep discharge cycles with a final capacity retention of 11% of original capacity (Figure S8).

The battery capacity varied rather much but the average specific capacity measured at 0.1 mA/cm^2 (excluding the large capacity cathode for TrGO3D) is reported in Table 2.

Table 2: The average specific capacity obtained in the Li-O_2 battery test for Super C65, HyrGO and TrGO cathodes (excluding the TrGO3D cathode of approximately 60,000 mAh/g).

Cathode	Binder content (%)	Average specific capacity/ mAh/g_{carbon}
Super C65	10	2922
HyrGO30min	10	4063
HyrGO3D	10	1457
TrGO30min	50	6947
TrGO3D	50	11038

This study shows that the TrGO cathodes have greater capacities than HyrGO cathodes, and that the HyrGO3D cathodes have an even lower capacity than the Super C65 cathodes. TrGO cathodes results in the highest capacity in the Li-O_2 battery of the tested cathode materials.

The difference in capacity between HyrGO and TrGO may be explained by general morphology difference or surface effects, since both TrGO samples are superior compared to the HyrGO cathodes. However, as HyrGO3D are of an even lower capacity than Super C65 cathodes, it may be that the C-N group leads to this decrease in capacity compared to TrGO cathodes. This would also be in agreement with HyrGO30min having a three times the capacity of HyrGO3D, even though the difference in C-N content is small. A comparison of the XPS results for TrGO30min and TrGO3D shows a decrease in the amount of C-C bonds and an increased ratio of edge groups, C(O)O and C=O. The decreased C-C ratio is not expected to be important and the C/O ratio do not seem to be of importance as no trend is observed. However, an increase in the ratio of C=O and C(O)O groups as well as an increased edge formation may serve as Li_2O_2 nucleation sites and introduce an increased Li_2O_2 coverage of the cathode. Since the highest capacity within the different reduced samples is reached by TrGO3D and HyrGO30min, respectively, it is possible that C=O, C(O)O and edge formation are less important for the capacity, and that something else is affecting it altogether. TrGO3D (484 m^2/g) has a larger surface area than to TrGO30min (342 m^2/g) and this might be the simple explanation for the difference in capacity. However, BET results for the HyrGO samples are rather similar: HyrGO30min 383 m^2/g and HyrGO3D of 399 m^2/g. If surface area was the defining capacity factor we would expect similar capacities for samples with similar surface area. All these assumptions are based on a capacity calculated from the amount of carbon material. However, if the capacity is calculated on cathode weight the results of TrGO30min would be similar to the

HyrGO30min. More definitive studies are needed but it is clear that the synthesis procedures of rGO and the initial GO samples are of immense importance for battery capacity.

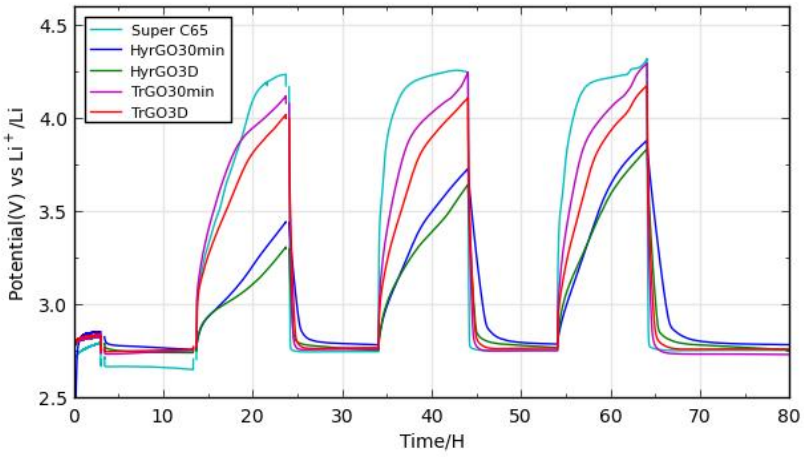

Figure 8: Limited battery test cycling curves for the five different cathodes displaying a difference in the potential reached for the time limited cycles dependent on material.

Figure 8 shows the time limited cycling from specific battery tests of the five different cathodes. This figure shows how the difference in cathode material results in significant differences in charging behavior and a possible smaller difference on discharge. It is clear that the charging voltage at a constant current has a more linear development for the HyrGO cathodes compared to the more steep curves of Super C65 and TrGO. The time dependent cycling of the battery shows that the HyrGO cathodes reach the time limit at a lower voltage. The TrGO cathodes result in a battery cycling which is more similar to super C65. However, the TrGO cathodes demonstrate a lower end potential and a 2nd and 3rd cycle which are not rising as steeply as the super C65 cathodes. The HyrGO cathodes showed the lowest overpotential with HyrGO30min and HyrGO3D being almost indistinguishable from one another. TrGO3D gives

the lowest end potential of the TrGO cathodes. The lower end potential for the HyrGO samples might be related to the C-N bonds on the surface, as this seems to be a definitive difference between the TrGO and HyrGO cathodes. However, other surface effects and morphology could also explain this. The small difference between TrGO30min and TrGO3D could be due to edge formation and edge functional groups. These results demonstrate that the time limited overpotential depends heavily on the cathode material. The cause of this difference might be that the functional groups make charge-transfer easier as well as surface and morphology effects may have a currently unknown influence. Conductivity of the cathodes might also affect the overpotentials, however in the review by Pei *et al* [16] the conductivity for a HyrGO material is 2 S/cm and the conductivity of TrGO in Schniepp *et al* [28] is between 10 and 23 S/cm. A low overpotential is important in Li-air batteries and much research is aimed toward optimizing this. If the battery material could be tailored to have a more efficient overpotential, the energy efficiency of the Li-air battery would be improved.

Another type of paint-casted cathode with an average area of 50 mm^2 was made and tested at 0.03mA/cm^2 for the TrGO30min and TrGO3D materials (50% PVDF). The cathodes had an average weight of 0.75 (30min) and 0.6 mg (3D) for the larger cathode area compared to the other type of cathodes, thus they were tested at a lower current per area but at a higher rate per mass materials. Three batteries of each type of material resulted in an average specific capacity of 3,734 mAh/g_{carbon} for TrGO30min and 23,757 mAh/g_{carbon} for TrGO3D. TrGO3D had the larger capacity for both types of cathodes. However, where the TrGO3D paint-casted cathode was superior in capacity compared to that of the drop-casted cathodes, the drop-casted cathodes were superior to the paint-casted for the TrGO30min samples. This signifies that the testing

conditions and preparation methods of cathodes as well as the material have to be considered in order to optimize the battery.

4. CONCLUSIONS:

The effect of oxidation time during synthesis of GO and the following chemically and thermally reduced GO was investigated. XRD of the GO sample showed an increased layer distance induced by oxidation time. XPS showed that the oxidation time of GO affects the ratio of functional groups on the graphene sheets. Part of these functional groups seemed to be extended to thermally and chemically rGO making the initial GO synthesis an important step before further reduction. ^{13}C MAS-NMR showed a small difference in the composition of GO30min and GO3D. In addition, the effect from the thermal reduction of GO to rGO clearly affects the ratio of the functional groups.

Cathodes of TrGOX and HyrGOX (X = 30min and 3D) were tested, and the highest capacity for a Li-O_2 battery today was reached with a TrGO3D cathode. It was furthermore possible to cycle batteries of TrGO3D and HyrGO3D, but only with significant capacity losses.

The high capacity combined with the ability to cycle is a very promising result for rGO based cathodes in Li-air batteries. The battery tests showed that the composition or the morphology of the rGO samples may have affecting the capacity, and that the different synthesis of the rGO resulted in very different batteries. The rGO synthesis method also affects time limited cycling yielding different shaped charging curves with different overpotentials for different cathodes. This study proved how rGO is a promising candidate for Li-air batteries of great capacity especially with a tailored rGO composition.

ACKNOWLEDGMENT:

The authors acknowledge support the ReLiable project funded by the Danish Council for Strategic Research−Programme Commission on Sustainable Energy and Environment (project no. 11-116792). StandUp for Energy is also gratefully acknowledged for support with funding.

ASSOCIATED CONTENT:

Supporting information is Available, containing data in regards to BET, TGA-MS, XRD, Raman and XPS is available free of charge online.

REFERENCES

[1] Girishkumar G, McCloskey B, Luntz AC, Swanson S, Wilcke W. Lithium−Air Battery: Promise and Challenges. J Phys Chem Lett. 2010;1(14):2193-203.
[2] Christensen J, Albertus P, Sanchez-Carrera RS, Lohmann T, Kozinsky B, Liedtke R, et al. A Critical Review of Li/Air Batteries. J Electrochem Soc. 2011;159(2):R1-R30.
[3] McCloskey BD, Bethune DS, Shelby RM, Girishkumar G, Luntz AC. Solvents' Critical Role in Nonaqueous Lithium–Oxygen Battery Electrochemistry. J Phys Chem Lett. 2011;2(10):1161-6.
[4] Younesi R, Norby P, Vegge T. A New Look at the Stability of Dimethyl Sulfoxide and Acetonitrile in Li-O2 Batteries. ECS Electrochem Lett 2014;3(3):A15-A8.
[5] Younesi R. Characterization of Reaction Products in the Li-O2 Battery Using Photoelectron Spectroscopy. University of Uppsala, Ph.D, 2012.
[6] Hummelshøj JS, Blomqvist J, Datta S, Vegge T, Rossmeisl J, Thygesen KS, et al. Communications: Elementary oxygen electrode reactions in the aprotic Li-air battery. J Chem Phys. 2010;132(7):071101.
[7] Chen J, Hummelshøj JS, Thygesen KS, Myrdal JSG, Nørskov JK, Vegge T. The role of transition metal interfaces on the electronic transport in lithium–air batteries. Catal Today. 2011;165(1):2-9.
[8] Mekonnen YS, Knudsen KB, Mýrdal JSG, Younesi R, Højberg J, Hjelm J, et al. Communication: The influence of CO2 poisoning on overvoltages and discharge capacity in non-aqueous Li-Air batteries. J Chem Phys. 2014;140(12):-.
[9] Gowda SR, Brunet A, Wallraff GM, McCloskey BD. Implications of CO2 Contamination in Rechargeable Nonaqueous Li–O2 Batteries. J Phys Chem Lett. 2013;4(2):276-9.

[10] Thotiyl MMO, Freunberger SA, Peng ZQ, Bruce PG. The Carbon Electrode in Nonaqueous Li-O-2 Cells. J Am Chem Soc. 2013;135(1):494-500.
[11] Ottakam Thotiyl MM, Freunberger SA, Peng Z, Chen Y, Liu Z, Bruce PG. A stable cathode for the aprotic Li–O2 battery. Nat Mater. 2013;12(11):1050-6.
[12] Shui J, Du F, Xue C, Li Q, Dai L. Vertically Aligned N-Doped Coral-like Carbon Fiber Arrays as Efficient Air Electrodes for High-Performance Nonaqueous Li–O2 Batteries. ACS Nano. 2014;8(3):3015-22.
[13] Lim H-D, Park K-Y, Song H, Jang EY, Gwon H, Kim J, et al. Enhanced Power and Rechargeability of a Li−O2 Battery Based on a Hierarchical-Fibril CNT Electrode. Adv Mater. 2013;25(9):1348-52.
[14] Xiao J, Mei D, Li X, Xu W, Wang D, Graff GL, et al. Hierarchically Porous Graphene as a Lithium–Air Battery Electrode. Nano Lett 2011;11(11):5071-8.
[15] Li Y, Wang J, Li X, Geng D, Li R, Sun X. Superior energy capacity of graphene nanosheets for a nonaqueous lithium-oxygen battery. Chem Commun. 2011;47(33):9438-40.
[16] Pei S, Cheng H-M. The reduction of graphene oxide. Carbon. 2012;50(9):3210-28.
[17] Li Y, Wang J, Li X, Geng D, Banis MN, Li R, et al. Nitrogen-doped graphene nanosheets as cathode materials with excellent electrocatalytic activity for high capacity lithium-oxygen batteries. Electrochem Commun. 2012;18(0):12-5.
[18] Li Y, Wang J, Li X, Geng D, Banis MN, Tang Y, et al. Discharge product morphology and increased charge performance of lithium-oxygen batteries with graphene nanosheet electrodes: the effect of sulphur doping. J Mater Chem. 2012;22(38):20170-4.
[19] Yang Y, Shi M, Zhou Q-F, Li Y-S, Fu Z-W. Platinum nanoparticle–graphene hybrids synthesized by liquid phase pulsed laser ablation as cathode catalysts for Li-air batteries. Electrochem Commun 2012;20(0):11-4.
[20] Dong S, Chen X, Zhang K, Gu L, Zhang L, Zhou X, et al. Molybdenum nitride based hybrid cathode for rechargeable lithium-O2 batteries. Chem Commun 2011;47(40):11291-3.
[21] Zhang W, Zeng Y, Xu C, Tan H, Liu W, Zhu J, et al. Fe2O3 nanocluster-decorated graphene as O2 electrode for high energy Li-O2 batteries. R Soc Chem Adv. 2012;2(22):8508-14.
[22] Wang LX, Ara M, Wadumesthrige K, Salley S, Ng KYS. Graphene nanosheet supported bifunctional catalyst for high cycle life Li-air batteries. J Power Sources. 2013;234:8-15.
[23] Yoo E, Zhou H. Li−Air Rechargeable Battery Based on Metal-free Graphene Nanosheet Catalysts. ACS Nano. 2011;5(4):3020-6.
[24] Mao S, Pu H, Chen J. Graphene oxide and its reduction: modeling and experimental progress. RSC Advances. 2012;2(7):2643-62.
[25] Zhu Y, Murali S, Cai W, Li X, Suk JW, Potts JR, et al. Graphene and Graphene Oxide: Synthesis, Properties, and Applications. Adv Mater. 2010;22(35):3906-24.
[26] Park S, An J, Piner RD, Jung I, Yang D, Velamakanni A, et al. Aqueous Suspension and Characterization of Chemically Modified Graphene Sheets. Chem Mater. 2008;20(21):6592-4.
[27] Stankovich S, Dikin DA, Piner RD, Kohlhaas KA, Kleinhammes A, Jia Y, et al. Synthesis of graphene-based nanosheets via chemical reduction of exfoliated graphite oxide. Carbon. 2007;45(7):1558-65.
[28] Schniepp HC, Li J-L, McAllister MJ, Sai H, Herrera-Alonso M, Adamson DH, et al. Functionalized Single Graphene Sheets Derived from Splitting Graphite Oxide. J Phys Chem B. 2006;110(17):8535-9.

[29] Zana A, Speder J, Reeler NEA, Vosch T, Arenz M. Investigating the corrosion of high surface area carbons during start/stop fuel cell conditions: A Raman study. Electrochim Acta. 2013;114(0):455-61.
[30] WaveMetrics IP, Version 4.0 IGOR Pro, Version 4.0.
[31] Morcombe CR, Zilm KW. Chemical shift referencing in MAS solid state NMR. J Magn Reson. 2003;162(2):479-86.
[32] Gao W, Alemany LB, Ci L, Ajayan PM. New insights into the structure and reduction of graphite oxide. Nat Chem. 2009;1(5):403-8.
[33] Williams D, Fleming I. Spectroscopic methods in organic chemistry, 5th edition: McGraw Hill; 1995
[34] McCloskey BD, Bethune DS, Shelby RM, Mori T, Scheffler R, Speidel A, et al. Limitations in Rechargeability of Li-O2 Batteries and Possible Origins. J Phys Chem Lett. 2012;3(20):3043-7.
[35] Blanton TN, Majumdar D. X-ray diffraction characterization of polymer intercalated graphite oxide. Powder Diff. 2012;27(02):104-7.
[36] Hiramitsu Y, Sato H, Hosomi H, Aoki Y, Harada T, Sakiyama Y, et al. Influence of humidification on deterioration of gas diffusivity in catalyst layer on polymer electrolyte fuel cell. J Power Sources. 2010;195(2):435-44.
[37] Tuinstra F, Koenig JL. Raman Spectrum of Graphite. J Chem Phys. 1970;53(3):1126-30.
[38] Ren P-G, Yan D-X, Ji X, Chen T, Li Z-M. Temperature dependence of graphene oxide reduced by hydrazine hydrate. Nanotechnology. 2011;22:055705.
[39] Yang D, Velamakanni A, Bozoklu G, Park S, Stoller M, Piner RD, et al. Chemical analysis of graphene oxide films after heat and chemical treatments by X-ray photoelectron and Micro-Raman spectroscopy. Carbon. 2009;47(1):145-52.
[40] Kim MC, Hwang GS, Ruoff RS. Epoxide reduction with hydrazine on graphene: A first principles study. J Chem Phys. 2009;131(6):064704.
[41] Panich AM, Shames AI, Sergeev NA. Paramagnetic Impurities in Graphene Oxide. Appl Magn Reson. 2013;44(1-2):107-16.
[42] Liu H, Zhang L, Guo Y, Cheng C, Yang L, Jiang L, et al. Reduction of graphene oxide to highly conductive graphene by Lawesson's reagent and its electrical applications. J Mater Chem C 2013;1(18):3104-9.